

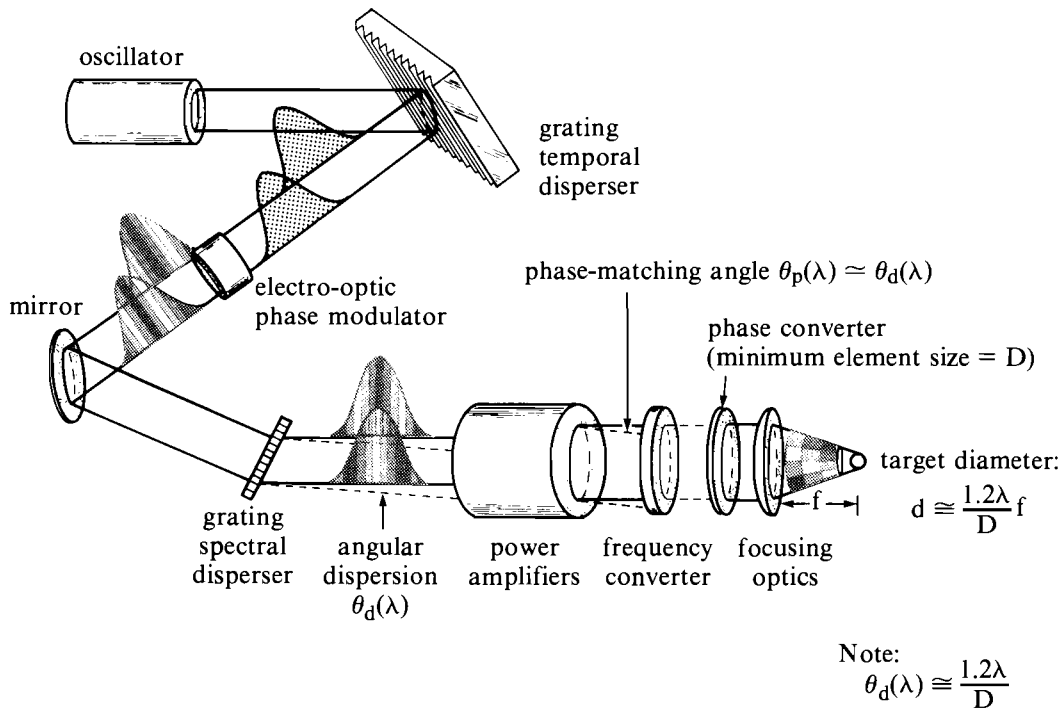
6. R. S. Craxton, S. D. Jacobs, J. E. Rizzo and R. Boni, *IEEE J. Quantum Electron.* **QE-17**, 1782 (1981).
7. M. Born and E. Wolf, *Principles of Optics*, 6th ed. (Pergamon Press, New York, 1980), pp. 403-406.
8. Ref. 7, pp. 436-437.
9. R. C. Eckardt and J. Reintjes, *IEEE Journal of Quantum Electron.* **QE-20**, 1178 (1984).

1.D Broadband Phase Conversion Using SSD

The propagation, amplification, and frequency conversion of broadband light in the OMEGA laser requires several system modifications. Figure 37.26 schematically represents the evolution of a laser beam throughout the system. The implementation of SSD in the OMEGA laser system includes the constraints that the group-velocity delay, electro-optic phase modulation, and angular dispersion be compatible with the current design. The majority of modifications are contained within the driver line where the smaller beam size and reduced energy level allow greater design flexibility. Phase conversion with distributed phase plates occurs at the end of each of the beamlines.

Broadband-Phase-Conversion Implementation

Laser beam parameters are best exploited early in a multibeam system, where the modifications are made only once. The driver line is easily modified to include new optical elements, holographic diffraction gratings, and a microwave phase modulator. Figure 37.27 illustrates the various changes that have been made to the OMEGA driver line. Two sets of kinematic mirror pairs are inserted into the straight beam path; one within the predriver zoom-relay and one just before the final 64-mm laser amplifier. In the predriver, various optical elements are situated between the kinematic mirrors to achieve lateral beam delay and bandwidth broadening. The output of the oscillator is spatially filtered, collimated, and expanded by a 5X keplerian telescope to produce a beam diameter of approximately 58 mm. Beam polarization is converted to linear "S" for efficient transfer through a three-element arrangement that contains one polarizer, a 57° transmission grating, and a second polarizer. The grating produces a lateral beam delay that is similar to the pulse width of the oscillator (650-ps FWHM). The associated angular spectral dispersion is ineffective since the oscillator is a Fourier-transform-limited narrow-band pulse. A second 5X telescope compresses the beam back to the original diameter. With an auxiliary positive lens, the beam is returned



E4716

Fig. 37.26

A new beam-smoothing technique—smoothing by spectral dispersion (SSD)—provides uniform target illumination for frequency-converted laser systems. The key technologies required for SSD are high-power holographic gratings, microwave phase modulators, and distributed phase plates.

to the zoom assembly with the correct numerical aperture for injection into the amplifier chain. A microwave-cavity phase modulator is positioned between the auxiliary lens and the zoom lens. Axial translation of the modulator allows the phase modulation to be introduced either in the near-field or the far-field. The latter is desired when electric-field nonuniformities or optical inhomogeneities exist within the electro-optic crystal. Free-propagation from the far-field can eliminate certain phase nonuniformities and spatially average the induced bandwidth. Air breakdown and crystal damage are prevented by limiting the value of the intermediate numerical apertures.

Lateral beam delay causes a certain amount of whole-beam nonuniformity in the near-field intensity distribution. In addition, a multifaceted grating is a source of edge diffraction. Together, these two sources of beam diffraction produce a deterioration of the far-field intensity distribution. Although these effects are well masked during phase conversion with distributed phase plates, the intermediate foci at the spatial filter pinholes contain an unwanted energy spread. For this reason, the spatial filter pinholes are enlarged throughout the driver line to prevent pinhole closure and near-field modulation.

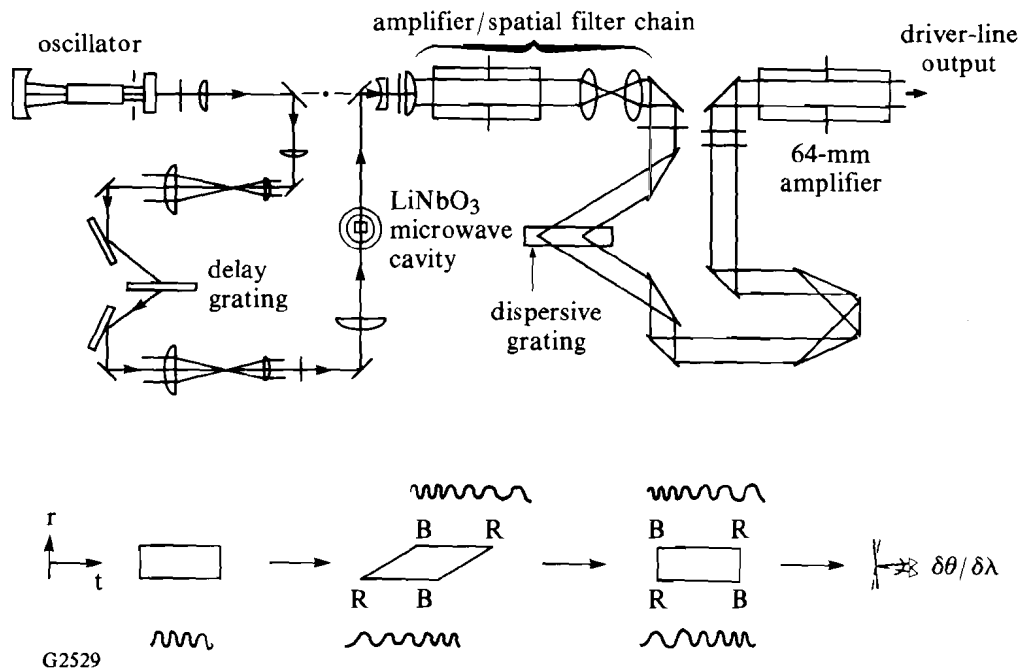


Fig. 37.27

Implementation of SSD on the OMEGA laser involves modification of only the driver line. Early in the driver line, one diffraction grating and the microwave phase modulator are appropriately positioned into an auxiliary beam path. The second grating is placed at the end of the driver line. Beam shaping, beam orientation, and polarization optical elements are included in both arms to achieve proper coupling of the beam parameters.

Removal of the lateral beam delay and addition of angular spectral dispersion are accomplished at the output of the driver line, just prior to the final 64-mm laser amplifier. As in the predriver, a polarizer-grating-polarizer arrangement is used to accommodate the relatively large angle of diffraction. The first diffraction grating is located at the hard-aperture image plane. The proper coupling of a Gaussian beam envelope with the high radial-gain profile from a series of rod amplifiers is preserved. Envelope distortion caused by diffraction is reduced with this choice of imaging. The second grating is located in a plane that is subsequently image relayed to a position outside the individual amplifiers throughout the 24 beamlines. Time-varying beam shifting occurs at these nonimage planes. It is anticipated that lateral beam shifting, on the spatial scale consistent with the peak growth for nonlinear beam-breakup, will offer a new mechanism for beam smoothing. Instantaneous nonlinear phase could be distributed over a spatial dimension to reduce the time-integrated intensity modulation below that which would occur if allowed to be spatially stationary.

As the beam propagates through the amplifier chain of the driver line, it has a constant lateral time delay and a time-varying spectrum

until it reaches the second grating. The angular spectral dispersion for this grating is set equal in magnitude but opposite in sign to the first grating to compensate for the lateral beam delay. This compensation restores the beam shape and creates a one-dimensional spectral gradient that also varies in time according to the modulation frequency of the microwave source. The two gratings must be oriented to provide the correct sign of angular spectral dispersion to the frequency-conversion crystals for proper phase matching of the individual spectral components. Angular demagnification between the driver line and the frequency-conversion cells is accounted for by over-dispersing the spectrum at the driver-line location.

The final step in broadband phase conversion is the propagation of broadband frequency-converted laser light through a distributed phase plate (DPP).¹ The time-varying spectral spread over one beam dimension samples the individual elements of the phase plates, thus producing a time-varying interference pattern. In addition, approximately 200 μrad of angular dispersion reaches the target chamber for a 2-Å spectral width. This translates to about a 10-mm ellipticity over a 165-mm-diameter beam for the extreme spectral components. Every point on the beam undergoes about a 10-mm sweep across the DPP at the rate of color modulation. The quickly varying interference pattern that results from this source of DPP sampling is another aspect of beam smoothing at the target plane.

Microwave Phase Modulator

The central device within the SSD system is a microwave phase modulator used to impress a time-varying bandwidth on the laser beam. Illustrated in Fig. 37.28, a resonant microwave cavity contains a rectangular crystal of lithium niobate. In order to achieve the modulation index required for SSD, between 4π to 6π , voltages of the order of tens of thousands of volts are required. A waveguide or strip-line approach with matched impedance geometry would require a high level of RF power (2 MW) to achieve 10 kV across a crystal. Since this is an excessively high power level, an alternative solution is required. A resonant cavity with a sufficiently high " Q " can generate high voltages for low-to-medium input power (2 kW).

The " Q " factor reduces the required input power in the following way. An RF voltage V , at the resonant frequency of the cavity, is applied with magnetic field coupling. For a cavity with a given Q , then after Q/π cycles of the microwave applied to the cavity, the voltage inside the cavity is $Q \times V$. At the frequencies of interest, in the 2- to 3-GHz region, it is straightforward to build cavities with Q 's of several thousand or several tens of thousands. With coupling efficiencies of several percent into the desired mode in the cavity, several tens of thousands of volts can be reached in several microseconds with power inputs of less than 2 to 3 kW.

In practice, the resonant frequency of the cavity depends heavily on the geometry of the crystal because of the very high dielectric constant of lithium niobate (23 at 2 GHz). This very high relative dielectric constant causes the lithium niobate to overwhelm the rest of the

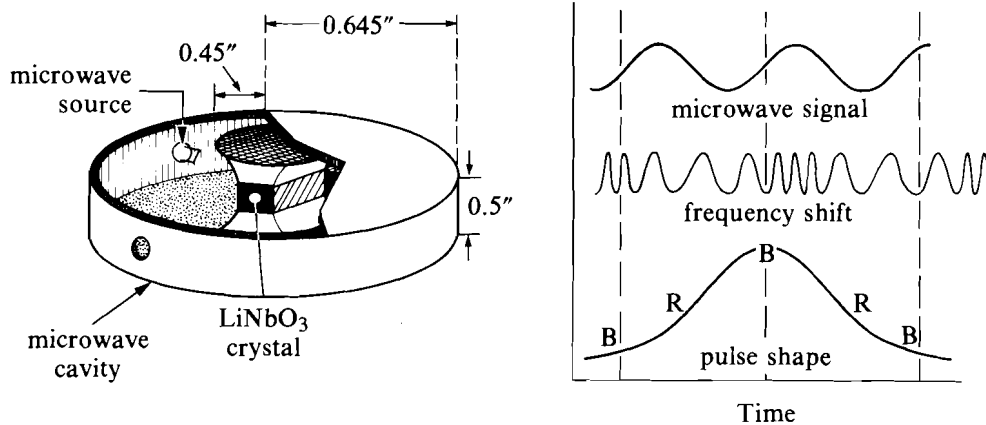
$$E(t) = e^{(i\omega t + i\eta \sin \omega_0 t)} = e^{i\omega t} \sum_{-\infty}^{\infty} J_n(\eta) e^{in\omega_0 t}$$

$$\omega_0 = 2\pi\nu_0$$

ν_0 - modulation frequency

η = modulation index

$$n_{\max} \sim \eta$$



G2472

Fig. 37.28

Electro-optic phase modulation is the source of spectral broadening. The phase modulator consists of a resonant radial-line cavity containing a crystal of lithium niobate. The microwaves are coupled-in through the magnetic field, producing electric-field amplification at the location of the crystal. Both the electric field and light polarization orient along the z axis of the crystal (perpendicular to the disc) for maximum phase modulation.

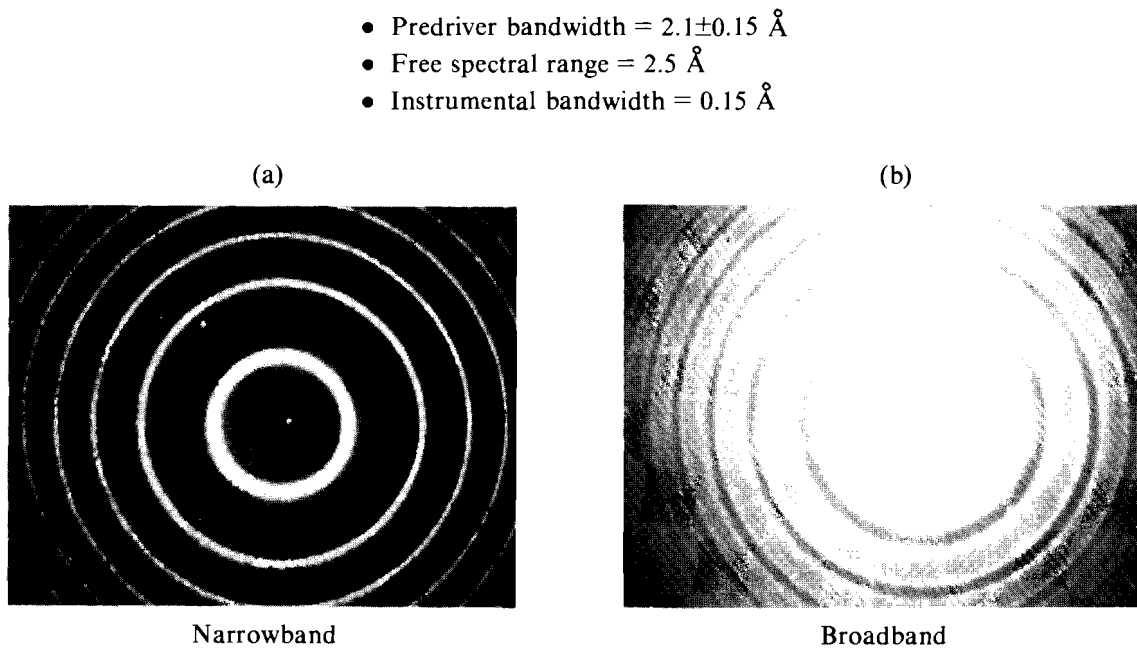
capacitive elements of the cavity and leads to a resonance much lower than that of the empty cavity.

Two specific cavity designs were tried in this experiment. Both were re-entrant designs where the crystal was placed in the gap between the re-entrant capacitive portion of the cavity and the ground plane of the cavity. Both coaxial resonators and radial-line resonators were designed and built. Because of its smaller dimensions, the radial-line-resonator approach was finally chosen. Without the crystal in the cavity, the resonant frequency was >3 GHz (the limit of our measuring equipment). With the crystal centered under the re-entrant post of the cavity, the frequency was lowered to 2.46 GHz. The Q , as measured to be in half-power points of the resonant frequency, was measured to be in excess of 10,000. Power was fed into the cavity through a sidewall-mounted loop probe of very small dimensions so as not to spoil the Q . The probe size was determined through a trade-off

between Q and coupling efficiency. With such high Q 's available, it was advantageous to use a very small probe with its attendant low coupling efficiency.

The RF power supply used to drive the cavity was a mechanically tuned, grid-pulsed, lighthouse tube cavity oscillator, which was capable of generating up to 5-kW pulses in 10- μ s pulses. With Q 's of the order of several thousand, complete voltage build-up occurred in the cavity (five e -folding times) in less than the pulse width. This allowed for some jitter in the rest of the timing electronics that synchronized the microwave pulser to the laser system.

Lithium niobate is oriented within the cavity with the Z-axis parallel to the re-entrant post axis. Phase modulation is achieved by polarizing the light parallel to these axes. The bandwidth is characterized with a Fabry-Perot interferometer. Figure 37.29 shows the spectral fringes before and after phase modulation. Bandwidth broadening is observed when the individual rings widen. In excess of 2 \AA of bandwidth is reproducibly achieved for laser shots on the OMEGA laser.



G2553

Fig. 37.29

Spectral measurements are made with a Fabry-Perot interferometer. Narrow-band radiation is characterized by narrow concentric rings whose separation represents the free spectral range. Bandwidth broadening is observed when the individual rings widen. A free spectral range of 2.5 \AA indicates a bandwidth of $\sim 2 \text{ \AA}$ for the data shown here.

High-Power Holographic Gratings

The base-line design, for the implementation of the simplified version of SSD, requires a group-velocity delay of about 600 ps both at the beginning and at the end of the driver line. An angular spectral dispersion of about $300 \mu\text{rad}/\text{\AA}$ at the output of the driver line is also required. Diffraction gratings can provide the required delay and dispersion, but there are additional performance requirements that must be fulfilled. The damage threshold of the grating at the end of the driver line must be $> 300 \text{ mJ}/\text{cm}^2$ at a pulse width of 650 ps (FWHM) for it to survive in a position just prior to the final 64-mm amplifier. The projected clear aperture of the grating must be slightly larger than the beam diameter. At an incident angle of 57° and a beam diameter of 58 mm the required grating dimension is about 130 mm. In addition, the grating must have a diffraction efficiency of $> 80\%$ while providing the correct angular dispersion.

Diffraction gratings can operate either in the reflection or transmission mode. Typically, a diffraction grating is characterized as a surface or volume and an amplitude or phase grating. A schematic of the surface-phase grating is shown in Fig. 37.30. A periodic, sinusoidal structure gives rise to diffraction according to the general grating equation,²

$$d [\sin(i) - \sin(\theta)] = m\lambda,$$

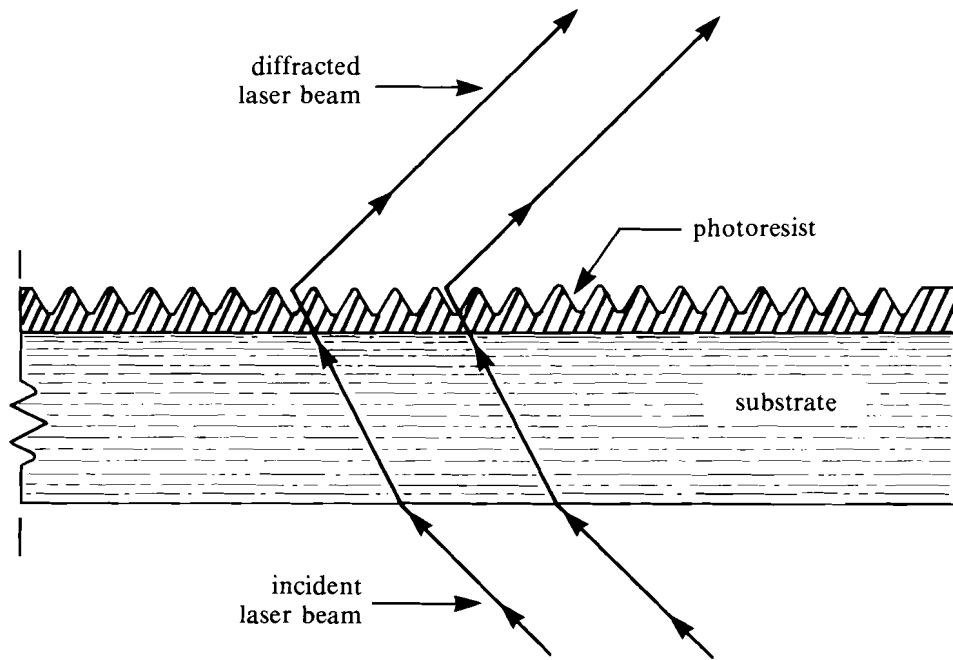
where d is the grating spacing, i is the angle of incidence, θ is the angle of diffraction, m is the diffraction order, and λ is the wavelength of light. The rate of change of the angle of diffraction with respect to wavelength, at a constant angle of incidence, is the definition of angular dispersion and is given by

$$\frac{\partial \theta}{\partial \lambda} = \frac{1}{d \cos(\theta)} .$$

The group-velocity path difference gives rise to the lateral-beam delay that is related to the beam diameter and the angle of incidence by

$$\Delta \tau = \frac{D[\tan(i) + \tan(\theta)]}{c} .$$

Table 37.I summarizes the diffraction grating design for the application of SSD in the OMEGA laser system.



G2556

Fig. 37.30

Holographic diffraction gratings used for SSD on OMEGA consist of a surface-relief layer of photoresist. High-power, high-efficiency gratings have for the first time been demonstrated at large apertures. Holotek, Ltd. (Rochester, NY) participated in the project by providing the holographic gratings.

Table 37.I
Diffraction grating design

Grating structure (d)	628 nm
Incident angle (i)	57°
Diffraction angle (θ)	57°
Order (m)	1
Wavelength	1054 nm
Angular dispersion (driver line)	$292 \mu\text{rad}/\text{\AA}$
Angular dispersion (conversion cells)	$100 \mu\text{rad}/\text{\AA}$
Lateral delay	585 ps

G2554

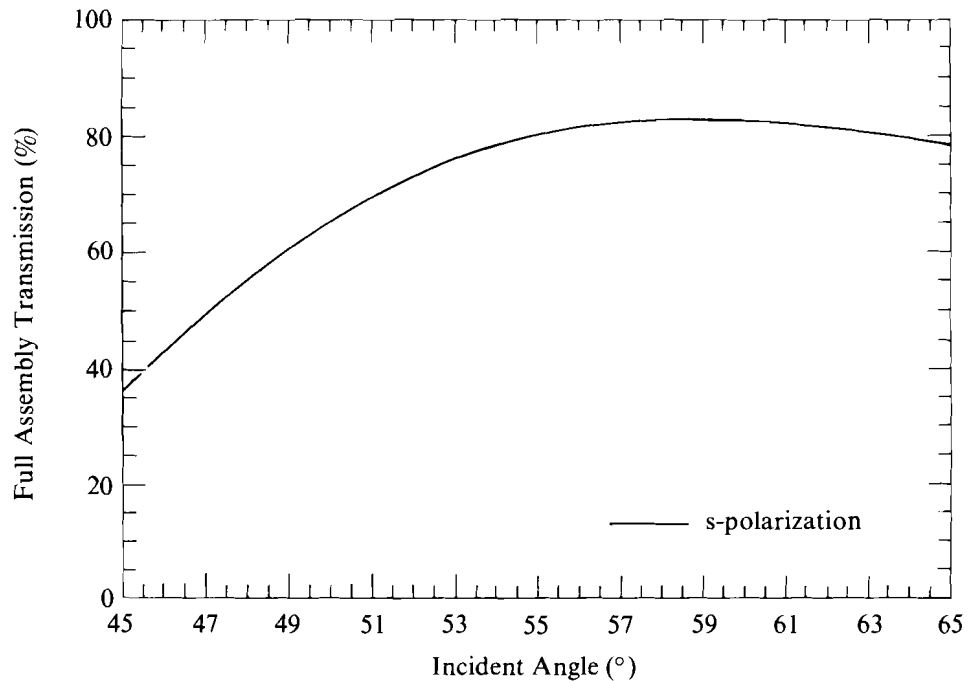
Several candidate materials have been investigated for use as high-power diffraction gratings.³ Ruled and holographic reflection gratings are generally overcoated with a metallic film to obtain high diffraction efficiency. However, metallic films intrinsically have a low damage threshold and cannot be used in high-power applications. Dichromated-gelatin, volume holograms have occasionally exhibited a high damage threshold, but this material is environmentally unstable and has not been scaled to a large-aperture, highly efficient optical component. There are several synthetic photopolymers that recently have been made available; however, very little is known about them with respect to high-power applications. Positive photoresist, the same material used in the manufacture of distributed phase plates, is currently the only successful material candidate. Holographic gratings made from photoresist are surface-relief phase gratings and therefore are used in the transmission mode.

High damage thresholds have been demonstrated for positive-photoresist master holograms that are fabricated at Holotek Ltd.⁴ An average 1-on-1 damage threshold of 0.8 J/cm^2 had made photoresist an attractive material early in the development stages. However, continued research revealed a hardening process in which fluence ramping over several laser shots increased the damage threshold. The N -on-1 damage threshold varied between 1.0 and 6.0 J/cm^2 at a pulse width of 650 ps and a wavelength of 1054 nm . Damage sites could not be produced at maximum system energy. As a result, two orders of magnitude greater fluence can be achieved when using diffraction gratings with high-power radiation.

Surface-relief gratings made from photoresist provide several other design advantages. Transmission diffraction efficiencies of $>85\%$ at $\lambda = 1054 \text{ nm}$ at $i = 57^\circ$ have been achieved with superior stability and very low noise. Furthermore, surface relief gratings possess a very broad angular response, providing alignment insensitivity and flexibility in selecting an angular spectral dispersion. Figure 37.31 shows the diffraction efficiency as a function of the incident angle for a grating that is sandwiched between antireflection-coated substrates. A full 10° angular range is available at negligible loss in efficiency. This performance applies only to "S" polarization, i.e., electric-field oscillation normal to the plane of incidence. Performance for "P" polarization can be increased, but only at the expense of S-polarization performance. Normally, obtaining high S-polarization efficiency is tantamount to achieving good polarization contrast.

In addition to beam smoothing by means of SSD, there are many applications for high-power diffraction gratings within a laser system. Gratings can be used as medium-contrast polarizers, multiwavelength beam splitters, spectroscopic elements, dispersive elements in an oscillator cavity, imaging elements, and spectral deflectors. Efficient frequency conversion, without requiring an angular dispersion to reach the target, can be achieved by placing diffraction gratings before and after the crystals. Another example involves the use of high-power gratings as the final optical element in several pulse-compression schemes.⁵

Further development of the surface-relief holographic grating, using either photoresist or photopolymer materials, can lead to higher diffraction efficiency at a larger clear aperture. Increasing the clear aperture of the grating is an important aspect of the current grating research. Size limitations depend primarily upon the deposition uniformity of the resist and the power and profile of the recording beams. Proper choice of the beam profiles can lead to successful continuous-wave or pulsed plane-wave holographic recording.⁶



*Grating fabrication provided by Holotek, Ltd.

G2557

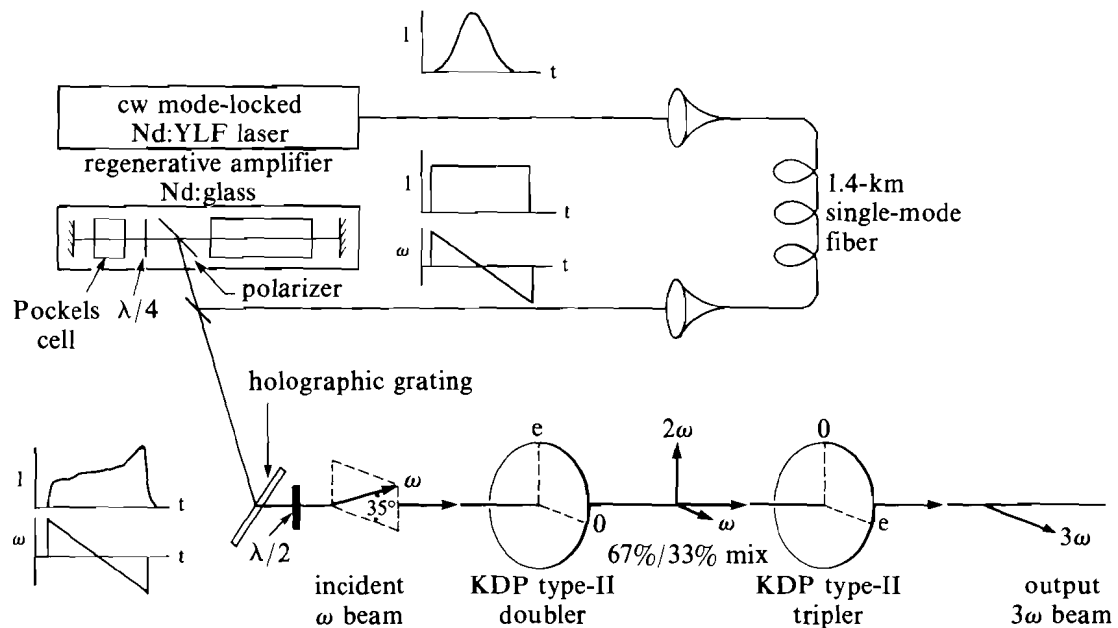
Fig. 37.31

The high-efficiency holographic gratings, provided by Holotek, Ltd., exhibit a broad angular response. The surface of the grating is sandwiched between two AR-coated glass plates for protection. The above curve shows a relatively constant diffraction efficiency for the assembly over 55°-65°.

Broadband Harmonic Conversion

In order to demonstrate that angular dispersion provides a means of frequency tripling broadband light, an experiment was performed using the setup illustrated in Fig. 37.32. The output of a Nd:YLF cw mode-locked laser was sent through 800 m of single-mode optical fiber to produce spectral broadening through self-phase modulation. Laser pulses exit the fiber at rate of 10^8 pulses per second, each pulse having a pulse width of 100 ps and a spectral bandwidth of ~ 25 Å. Due to the positive group-velocity dispersion in the fiber, the frequency components are dispersed in time in such a way that the

long wavelengths emerge from the fiber ahead of the shorter wavelengths. A single pulse from the fiber was then amplified in a Nd:glass regenerative amplifier. The amplifier cavity included a 50% reflecting-output coupler, producing a 15-pulse envelope that contained ~ 7 mJ. The entire pulse train was used for the broadband frequency-tripling experiment. The experiment consisted of two configurations: one with and one without angular spectral dispersion.



G2558

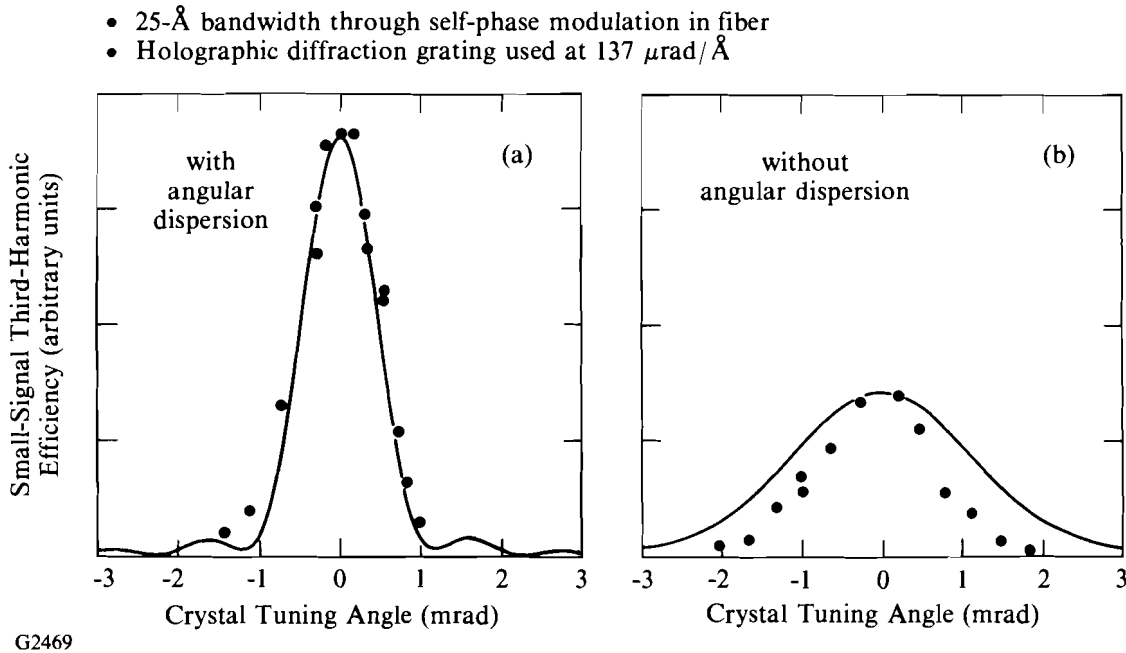
Fig. 37.32

The experimental setup used to study broadband frequency tripling included a cw mode-locked Nd:YLF laser source that was fiber-optically coupled to a Nd:glass regenerative amplifier. 25 Å of spectral broadening was generated through 800 m of fiber and maintained within the regenerative amplifier. The broadband radiation was harmonically converted through a KDP crystal, using the angular dispersion made available by the holographic gratings.

For the case when angular spectral dispersion was impressed on the input wave, the grating was oriented so that the plane of dispersion contained the e -axis of the tripling crystal. The source of dispersion was a Holotek⁴ photoresist, holographic "Master" grating. The periodic structure of the grating had a spacing of about 1.1 μm and was used at 45° to produce an angular spectral dispersion of 137 $\mu\text{rad}/\text{Å}$. The beam was then passed through a polarizer to set the polarization required for optimum harmonic generation. The beam intensity was adjusted by way of a half-wave plate located before the polarization-sensitive diffraction grating. The second-harmonic converter was a 1.6-cm KDP crystal oriented with its optic axis in the y - z plane. The

optic axis of the doubling crystal was adjusted so that the phase-matching condition was satisfied by the center frequency of the input laser. Since the angular dispersion of the input wave was in the x - z plane, the frequency components of the input beam are effectively all o rays within the doubler and are insensitive to small angular changes. The second-harmonic signal then exits the crystal polarized in the y -direction and is mixed with the residual fundamental radiation in another 1.6-cm KDP crystal. The third-harmonic generation crystal was oriented with its optic axis in the x - z plane so that the angular dispersion impressed on the input wave matched the acceptance angle of the tripler ($166 \mu\text{rad}/\text{\AA}$).

The experiment measured the intensity of the third-harmonic signal as a function of the tuning angle, with and without angular dispersion from the high-power grating. The results are displayed in Fig. 37.33. The intensity of the third-harmonic signal increased by greater than a factor of 2.5 for the case when angular dispersion was impressed on the input beam.



G2469

Fig. 37.33

For the first time, optimum third-harmonic generation of broadband light was demonstrated using angular spectral dispersion. Without angular dispersion, the tripler efficiency is relatively insensitive to tuning angle. Tripler efficiency substantially increases with the addition of an angular dispersion that approaches the wavelength mismatch in the KDP tripling crystal.

SSD Demonstration on OMEGA

Broadband phase conversion using SSD has recently been fully implemented on the OMEGA laser system. A wide range of diagnostics was deployed to demonstrate the benefits of SSD, both for

the fusion target and the laser system. Figure 37.34 is a comparison of the equivalent-target-plane intensity distributions for normal focusing (a), phase-converted focusing (b), and broadband phase conversion using SSD (c). Phase conversion with the distributed phase plates produces a well-defined envelope and shifts the intensity-power spectrum toward high spatial frequencies. SSD smooths these higher spatial frequencies and reduces the modulation of the lower spatial frequencies at the same time.

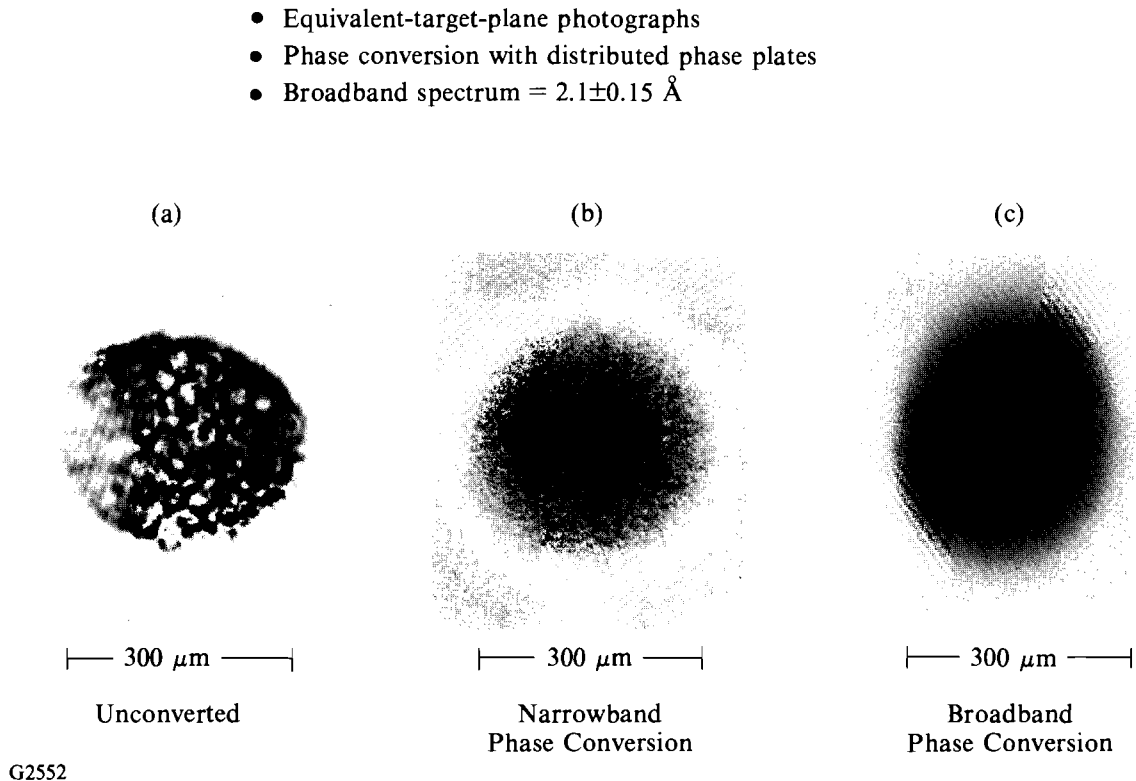
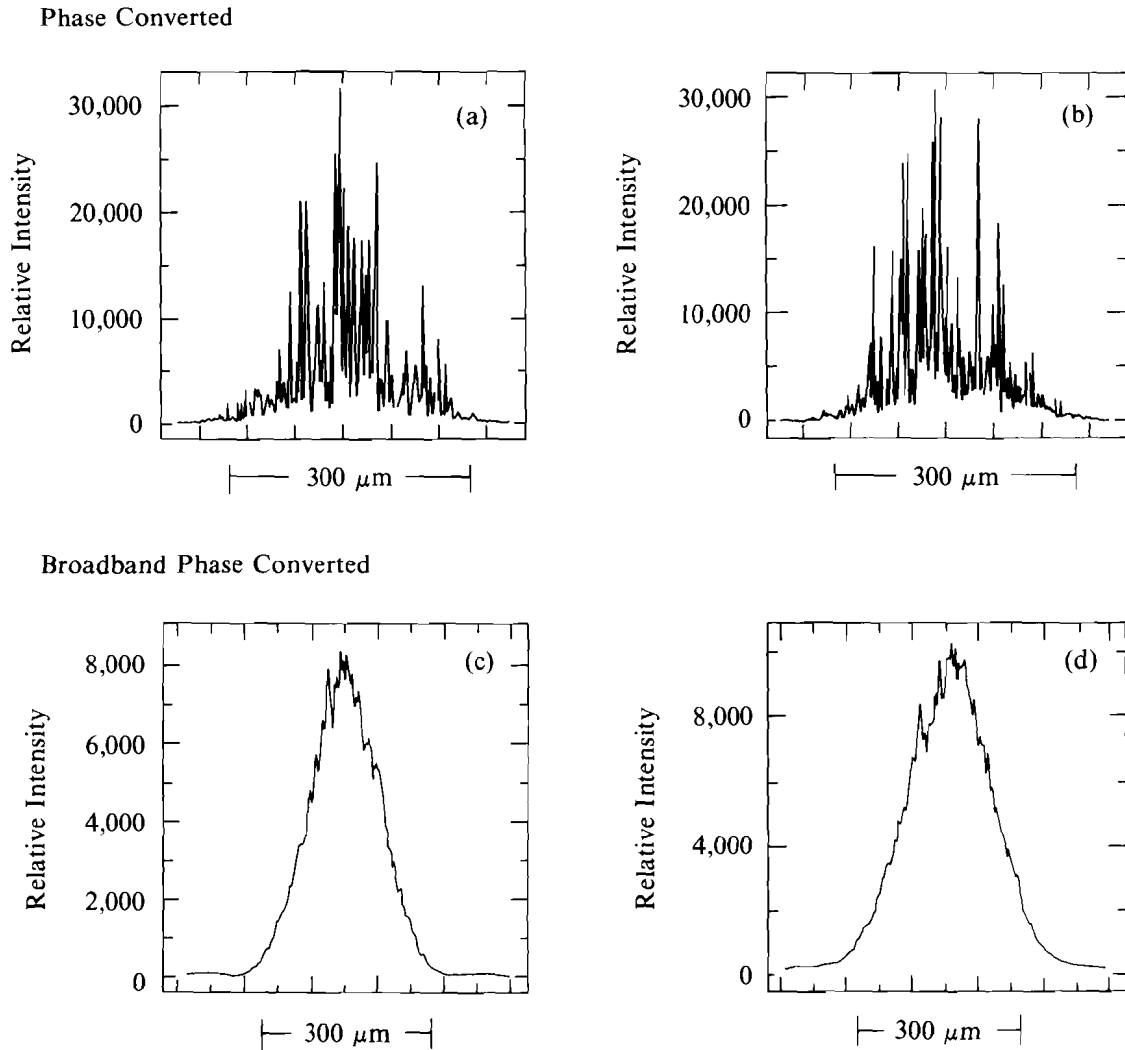


Fig. 37.34

Equivalent-target-plane photography shows dramatic improvements in the focal beam quality after implementing SSD on the OMEGA laser. Normal focusing of frequency-tripled laser light shows hot-spot intensity features (a). The distributed phase plates (DPP's) provide a well-defined envelope and an insensitivity to near-field wave-front errors (b). Spectral dispersion provides a substantial smoothing of the structure produced by the phase plate (c).

The resulting intensity distributions are smooth enough to require diligent cleaning and calibration of the photographic diagnostics. Figure 37.35 is a comparison of cross sections of intensity for phase conversion with and without SSD. The cut-off spatial frequency, corresponding to $3 \mu\text{m}$, is fully sampled for the data. Therefore, no amount of smoothing is assumed for these representations of the equivalent target plane. It is clear from the comparison that substantial smoothing has been achieved in both directions: parallel and

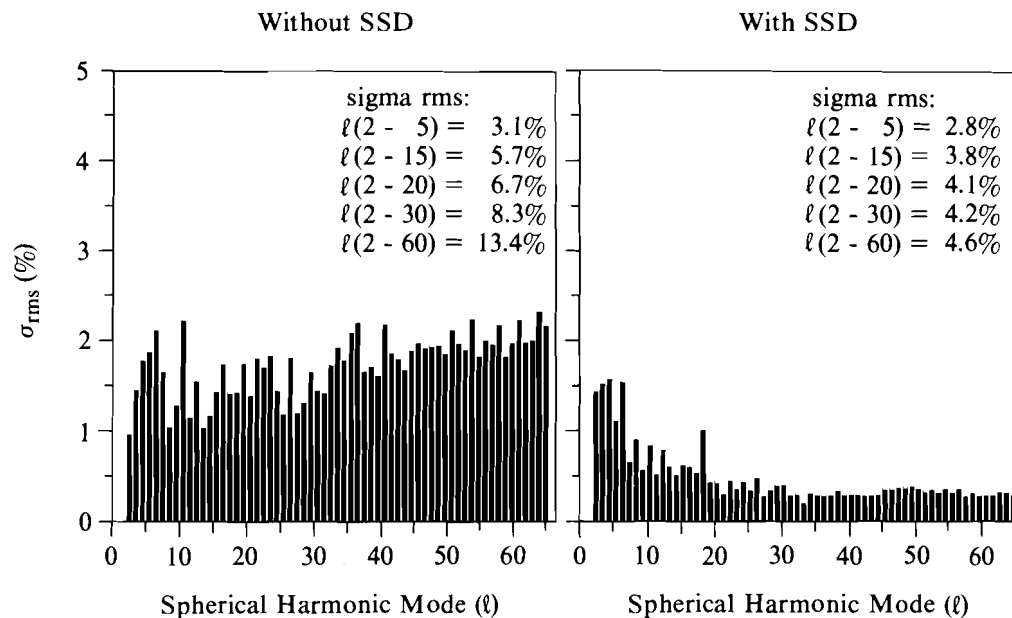


G2555

Fig. 37.35

Cross sections of the intensity distribution show a high level of beam smoothing by SSD. The cross sections are resolved to the limiting spatial frequency corresponding to $3 \mu\text{m}$. Smoothing is observed in both dimensions: parallel and perpendicular to the direction of spectral dispersion.

perpendicular to the axis of spectral dispersion. Accurate assessment of the benefit from 24 smooth laser beams is obtained by a computer calculation that involves beam superposition about a sphere and an ℓ -mode decomposition of the resulting intensity distribution. Figure 37.36 shows a substantial decrease in the amplitude of all of the ℓ -modes, indicating a significant improvement in irradiation uniformity for the OMEGA laser system.



*Beams smoothed over 1% of the beam radius

TC2552

Fig. 37.36 Superposition of the 24 OMEGA focal distributions shows a substantial improvement in irradiation uniformity. The l -mode decompositions show greater than a factor-of-4 times lower nonuniformity when using SSD.

Additional beam smoothing has been demonstrated from free-space propagation between the frequency-conversion crystals and the target chamber. Furthermore, a more optimum envelope from each of the individual laser beams is achieved by operating the distributed phase plates out of the exact Fourier plane.

Conclusion

A novel beam-smoothing technique—smoothing by spectral dispersion (SSD)—has been successfully implemented on the OMEGA laser system. The integration of a large-aperture, high modulation-index, microwave phase-modulator and high-power, high-efficiency, holographic diffraction gratings has made it possible to manipulate a beam’s spectral distribution in time and space. Substantial improvement in the uniformity of irradiation from the OMEGA laser has been demonstrated.

ACKNOWLEDGMENT

This work was supported by the U.S. Department of Energy Office of Inertial Fusion under agreement No. DE-FC03-85DP40200 and by the Laser Fusion Feasibility Project at the Laboratory for Laser Energetics, which has the following sponsors: Empire State Electric Energy Research Corporation, New York State Energy Research and Development Authority, Ontario Hydro, and the University of Rochester. Such support does not imply endorsement of the content by any of the above parties.

REFERENCES

1. LLE Review **33**, 1 (1987).
2. M. Born and E. Wolf, *Principles of Optics*, 6th ed. (Pergamon Press, NY, 1980), pp. 401–414.
3. H. M. Smith, *Holographic Recording Materials* (Springer-Verlag, Berlin, 1977), pp. 209–226.
4. Holotek LTD., Holotek products literature, August 1984, pp. 4–5.
5. D. Strickland and G. Mourou, “Compression of Amplified Chirped Optical Pulses,” *Opt. Commun.* **56**, 219 (1985).
6. T. J. Kessler, M. S. thesis, The Institute of Optics, University of Rochester, 1984.